AGU ADVANCING EARTH AND SPACE SCIENCES

AGU Advances

RESEARCH ARTICLE
10.1029/2024AV001379

Peer Review The peer review history for this article is available as a PDF in the Supporting Information.

Key Points:

- SYISR and GEO total electron content network were first used to analyze unique ionospheric changes to the May 2024 superstorm over the Asian sector
- Disturbed meridional winds modulated by atmospheric gravity waves (AGWs), strong upward ion drift oscillations and large downward ion drifts occurred on superstorm day
- The interplay of AGWs and disturbance electric fields results in abnormal stormtime ionospheric variations

Supporting Information:

Supporting Information may be found in the online version of this article.

Correspondence to:

J. Lei and X. Yue,
leijh@ustc.edu.cn;
yuexinan@mail.iggcas.ac.cn

Citation:

Huang, F., Lei, J., Yue, X., Li, Z., Zhang, N., Cai, Y., et al. (2025). Interplay of gravity waves and disturbance electric fields to the abnormal ionospheric variations during the 11 May 2024 superstorm. *AGU Advances*, *6*, e2024AV001379. https://doi.org/10.1029/2024AV001379

Received 1 JUL 2024
Accepted 26 JAN 2025

Author Contributions:

Conceptualization: Fuqing Huang, Jiuhou Lei
Data curation: Fuqing Huang, Xinan Yue, Ning Zhang, Yihui Cai, Yihan Wang, Jiahao Zhong
Formal analysis: Fuqing Huang
Funding acquisition: Jiuhou Lei
Investigation: Fuqing Huang, Zhongli Li, Shun-Rong Zhang, Xiaoli Luan

Interplay of Gravity Waves and Disturbance Electric Fields to the Abnormal Ionospheric Variations During the 11 May 2024 Superstorm

Fuqing Huang[1,2,3], Jiuhou Lei[1], Xinan Yue[4,5], Zhongli Li[1], Ning Zhang[4,5], Yihui Cai[4,5], Shun-Rong Zhang[6], Yihan Wang[1], Jiahao Zhong[7], and Xiaoli Luan[1]

[1]Deep Space Exploration Laboratory/School of Earth and Space Sciences, University of Science and Technology of China, Hefei, China, [2]CAS Center for Excellence in Comparative Planetology/CAS Key Laboratory of Geospace Environment/Mengcheng National Geophysical Observatory, University of Science and Technology of China, Hefei, China, [3]Collaborative Innovation Center of Astronautical Science and Technology, Harbin, China, [4]Key Laboratory of Earth and Planetary Physics, Institute of Geology and Geophysics, Chinese Academy of Sciences, Beijing, China, [5]Beijing National Observatory of Space Environment, Institute of Geology and Geophysics, Chinese Academy of Sciences, Beijing, China, [6]Haystack Observatory, Massachusetts Institute of Technology, Westford, MA, USA, [7]Planetary Environmental and Astrobiological Research Laboratory (PEARL), School of Atmospheric Sciences, Sun Yat-sen University, Zhuhai, China

Abstract The strongest geomagnetic storm in the preceding two decades occurred in May 2024. Over these years, ground-based observational capabilities have been significantly enhanced to monitor the ionospheric weather. Notably, the newly established Sanya incoherent scatter radar (SYISR) (Yue, Wan, Ning, & Jin, 2022, https://doi.org/10.1038/s41550-022-01684-1), one of the critical infrastructures of the Chinese "Meridian Project," provides multiple parameter measurements in the upper atmosphere at low latitudes over Asian longitudies. Unique ionospheric changes on superstorm day 11 May were first recorded by the SYISR experiments and the geostationary satellite (GEO) total electron content (TEC) network over the Asian sector. The electron density or TEC displayed wavelike structures rather than a regular diurnal pattern. Surprisingly, two humps, a common feature in the daytime equatorial ionization anomaly structure, disappeared. The SYISR observations revealed that multiple wind surges accompanied the downward phase propagation caused by atmospheric gravity waves (AGWs) originating from auroral zones. Meanwhile, strong upward and large downward drifts were respectively observed in the daytime and around sunset. The Thermosphere-Ionosphere Electrodynamics Global Circulation Model (TIEGCM) simulations demonstrated that abnormal ionospheric changes were attributed to meridional wind disturbances associated with AGWs and recurrent penetration electric fields corresponding to larger B_z southward excursions and disturbance dynamo. The complicated interplay between AGWs and disturbance electric fields contributed to this unique ionospheric variation.

Plain Language Summary During a geomagnetic storm, the ionosphere-thermosphere system undergoes severe disturbances, seriously affecting satellite orbits and radio propagation. Since the Halloween superstorm in October 2003, the most intense storm occurred in May 2024, with the ring current index *Dst* dropping below −400 nT. Unlike 20 years ago when limited observations were available, China has now established a comprehensive ground-based observation network, known as the "Meridian Project." This project aims to monitor the ionospheric weather over the Chinese sector. The Sanya ISR, one of the critical infrastructures of this project, provides multiple parameter measurements in the upper atmosphere. With the robust ISR observations, we found that unique ionospheric changes happened in the upper atmosphere in response to this superstorm. Moreover, the model simulations are also utilized to understand physical processes during the severe geomagnetic storm toward the space weather forecast.

1. Introduction

It is well known that massive energy and momentum transferred from solar winds can cause major disturbances in chemical, dynamical, and electrodynamical processes in the ionosphere and thermosphere system (I-T System) during storms (Gonzalez et al., 1994; Prölss, 1995; Richmond & Lu, 2000). They will produce severe changes in electron density and neutral density affecting satellite and spacecraft orbits and radio propagation or even causing signal interruptions (e.g., Coster et al., 2021; Dang et al., 2022; McNamara, 1991; Skone & Yousuf, 2007).

Methodology: Fuqing Huang, Xinan Yue, Zhongli Li, Ning Zhang, Yihan Wang
Project administration: Jiuhou Lei
Resources: Fuqing Huang, Jiuhou Lei
Software: Fuqing Huang, Zhongli Li
Supervision: Jiuhou Lei, Xiaoli Luan
Validation: Fuqing Huang
Writing – original draft: Fuqing Huang
Writing – review & editing: Fuqing Huang, Jiuhou Lei, Xinan Yue, Ning Zhang, Yihui Cai, Shun-Rong Zhang, Xiaoli Luan

How these disturbances affect ionospheric variations has been extensively studied (e.g., C.-S. Huang et al., 2005; Lei et al., 2008; Lin et al., 2005; Mannucci et al., 2008; W. Wang et al., 2010). For instance, during interplanetary magnetic field (IMF) B_z southward excursions, the prompt effects of penetrating electric fields can result in daytime electron density or total electron content (TEC) enhancement, even generating superbubbles at low latitudes (Lei et al., 2008; Lin et al., 2005; Ma & Maruyama, 2006; W. Wang et al., 2010). The neutral wind disturbances associated with traveling atmospheric disturbances (TADs), which are atmospheric gravity waves (AGWs) produced via enhanced Joule heating during geomagnetic disturbances (Richmond & Roble, 1979), can also lead to ionospheric changes. These changes can transport plasma along field lines, affect the E and F region wind dynamo and potentially seed for plasma bubbles (e.g., Jin et al., 2022; Liu & Vadas, 2013; Prölss, 1993, 1995). However, the relative effects of penetrating electric fields, neutral wind disturbances, and other factors and their interactions during storms are not yet fully understood (Buonsanto, 1999; Mendillo, 2006). The complicated interactions among these processes are the major causes of complicated ionospheric responses to storms.

A significant limitation is the observation deficiency, particularly the simultaneous measurements of multiple parameters such as thermospheric winds and electric fields. This issue is especially pronounced in Asia, where comprehensive observations are lacking in the past. For instance, Buonsanto (1999) noted that "How TEC changes during storms might be driven by winds remains a premier observational challenge," Mendillo (2006) questioned "Are there observations that can help us understand the persistent dual maxima in TEC storm," and Luan (2021) emphasized that "The simultaneous measurements between thermospheric winds and electric fields are important for verifying and improving the current understanding of the equatorial ionization anomaly (EIA) variations and the dynamics and electrodynamics involved during the storms."

The Sun entered a period of high-level activity since 2023, and a super geomagnetic storm erupted in May 2024. This storm is currently the strongest one in the last 20 years. There was a prominent fluctuation in the IMF B_z component varying between the northern and southern directions. The maximum B_z values ranged from ∼−25 nT to ∼−50 nT. The geomagnetic activity index *Dst* dropped to a minimum value lower than −400 nT. Fortunately, China recently established the "Meridian Project," which offers comprehensive ground-based observations (C. Wang et al., 2023, 2024). These observations provide an excellent opportunity to monitor the upper atmosphere and ionosphere during this superstorm event. And they are also crucial for validating theoretical models. Combining these observations helps to enhance our understanding of the upper atmosphere's response to geomagnetic storms and improve model performance.

In this study, we utilized the newly built Sanya incoherent scatter radar (SYISR), a crucial component of the Chinese Meridian Project, to first analyze abnormal ionosphere variations during the superstorm on 11 May 2024. By combining TEC data from the Chinese Beidou and Japanese geostationary satellites (GEO) over the Asian sector, as well as model simulations, the abnormal ionosphere variations induced by the superstorm and the possible physical mechanisms are systematically investigated.

2. Data Set and Methods

The Global Navigation Satellite System (GNSS) GEO TEC and SYISR multiparameter data were used in this study. GEO TECs with a temporal resolution of 30 s from 52 GNSS receivers over South Asia were used. Forty of these stations are from the Beidou Ionospheric Monitoring Network built by the University of Science and Technology of China (USTC), and the others are from the international GNSS service (IGS) network. The GEO satellites, with motionless ionospheric pierce points (IPPs), provide more reliable TEC observations than non-GEO satellites (e.g., GPS satellites), since the TEC observed by non-GEO satellites is known to be contaminated by spatial variations due to satellite motion (F. Huang et al., 2017, 2018, 2023). This study used the Chinese Beidou and Japanese GEO satellite TEC observations with IPPs located at ∼110° ± 2.5°E to analyze abnormal ionospheric variations on superstorm day. Detail about these GNSS stations and the associated GEO satellites is given in Figure S1 and Table S1 in Supporting Information S1. Combined with GEO TEC data, the ISR observed electron density, line-of-sight (LOS) ion velocity, meridional winds, and vertical ion drifts over Sanya (109.6°E, 18.3°N, magnetic latitude: (MLAT) 11.55°N), were first employed to investigate dynamic processes during the abnormal ionospheric variation periods. These ISR parameters were observed from 11 beams along and perpendicular to the magnetic meridian plane (Yue, Wan, Ning, Jin, et al., 2022). Each beam integrates for 30 s, and results in a temporal resolution of 5.5 min for each parameter. The meridional winds and vertical ion drifts were derived from LOS velocities observed by multiple beams in different directions (Zhang et al., 2024). As

Table 1
Basic Modules for O^+ Solver (Column 2), Dynamo Solver (Column 3), O^+ Output (Column 4), and Corresponding Note (Column 5) for Different TIEGCM Runs (Column 1)

	O^+ solver		Dynamo solver			
Run	*Oplus.F*	*Oplus_new.F*	*Pdynamo.F*	*Pdynamo_new.F*	O^+ output	Note
1	√		√		*Oplus.F*	Default run
2	√	√, meridional winds on 9 May from Run 1	√		*Oplus_new.F*	Meridional wind dynamic effect: Run 2–Run 1
3	√	√, vertical drifts on 9 May from Run 1	√		*Oplus_new.F*	Vertical drift effect: Run 3–Run1
4	√	√, electric fields from the module *Pdynamo_new.F*	√	√, neutral winds on 9 May from Run 1	*Oplus_new.F*	Disturbance dynamo effect: Run 4–Run 1

Note. √ represents the module used for TIEGCM runs for this storm event. The *Oplus_new.F and Pdynamo_new.F* are an additional module for O^+ solver and Dynamo solver, respectively, which run together with the full model simulation.

outlined in Zhang et al. (2024), the vector velocity is first determined through the least squares fitting procedure using the SYISR LOS velocity measurements in different directions. Electric fields as well as vertical and parallel ion drifts can be accordingly derived, and meridional winds are further determined following the ion diffusion velocity calculation. In this work, to derive meridional winds and vertical ion drifts in the F-region, the SYISR 11-beam LOS velocities are observed in two special planes: One is in the geomagnetic meridian with elevation angles of 45°, 60°, 75°, 90°, 75°, 60°, and 45° and the other is in the plane perpendicular to the meridional one with elevation angles 60°, 75°, 90°, 75°, and 60°.

Moreover, we carried out simulations to further analyze the dynamics and electrodynamic behavior during the May 2024 superstorm, using the first-principles model of the Thermosphere-Ionosphere Electrodynamics Global Circulation Model (TIEGCM). This model has a high resolution of 2.5° × 2.5° in latitude and longitude in the geographic coordinates. The Weimer model (Weimer, 2005), which is driven by the observed solar wind and IMF parameters, specifies the high latitudinal electric potential in the TIEGCM. Therefore, the prompt penetration electric field (PPEF) primarily penetrates from high latitudes without significant attenuation to low and middle latitudes, and the disturbance dynamo takes effect at later times (Lei et al., 2018; W. Wang et al., 2008). In order to analyze the relative effects of the PPEF, disturbance dynamo, and meridional winds on the ionospheric variations during this superstorm, we conducted controlled runs (Dang et al., 2016). To examine the respective contribution of each parameter to the ionospheric variations, in the simulations, we added three new modules in which the meridional winds, vertical $E \times B$ drifts, and disturbance dynamo were replaced by those from quiescent conditions (9 May 2024) respectively while the coupling and interaction processes are preserving in the I-T System (including unchanged thermospheric composition).

The detailed settings for the TIEGCM runs are listed in Table 1. First, we conducted the default TIEGCM simulation (Run 1), in which the original modules *Oplus.F* and *Pdynamo.F* correspond to the O^+ solver and dynamo solver, respectively. Then, we carried out three controlled runs, in which the new parallel modules (*Oplus_new.F* and *Pdynamo_new.F*) are used, but their outputs were not fed back into the original simulation.

Specifically, in the controlled run for meridional effect (Run 2), the new module *Oplus_new.F* is generally the same as the original one *Oplus.F*, and these two modules (*Oplus_new.F and Oplus.F*) solve O^+ equation and calculate the electron density independently. In the module *Oplus_new.F*, the meridional winds from Run 1 are used on the reference day. Similarly, in Run 3, the vertical $E \times B$ drifts simulated from Run 1 on the reference day are used as input in the new module *Oplus_new.F*. In Run 4, the new module *Oplus_new.F* uses the electric fields obtained from the module *Pdynamo_new.F*, which takes the neutral winds from Run 1 on the reference day. Subsequently, the differential TEC values between the control runs (Runs 2–4) and Run 1 are calculated to assess the storm effect of meridional winds, vertical drifts, and disturbance dynamo on the ionospheric changes, respectively. Given that the entire thermosphere and ionosphere system is coupled, this control simulation strategy impossible to independently distinguish the effects due to the inherent nature of the coupling. Nevertheless, these simulations can provide reasonable estimations of the contributions of dynamic and electrodynamic drivers to ionospheric changes during this superstorm.

3. Results and Discussions

Figures 1a and 1b show the daily variations in electron density and LOS velocity from the SYISR zenith beam experiment on the superstorm day of 11 May 2024. When the quiescent day on 13 May 2024 (as a reference) shown in Figure 2 was compared, the observed electron density changes were unique with abnormal variation at the F2 layer altitudes. On the reference day, the electron density peak was exhibited in the afternoon and a trough occurred in the post-midnight period at F2 layer altitudes, thus the electron density displayed typical diurnal variations. However, on the superstorm day, the electron density had multiple peaks at approximately 01:30, 04:30, 10:00, and 11:00 UT, displaying wavelike structures. The F2 layer peak height (hmF2) also had corresponding wavelike structures. Meanwhile, the storm-time LOS velocities showed distinct features compared to those of the reference observations (Figure 2b). The reference ones did not show significant fluctuations for both the upward and downward movements, and the upward component was larger during the period from sunrise to noon and the downward one was stronger from after sunset to before sunrise. The LOS velocity changed directions several times and had an amplitude of ∼100 m/s between 00:00 and 13:00 UT on the superstorm day. Additionally, downward phase propagation was observed in the LOS velocity of different directions.

We further examined the critical dynamic parameters of meridional winds and vertical plasma drifts, which were simultaneously derived from the SYISR LOS velocities over the Chinese sector for the first time. The two parameters were shown in Figures 1c and 1d to analyze their relative effects on ionospheric variations during the superstorm. These two are the main factors controlling changes in the ionospheric electron density at the equator and low latitudes due to the plasma transport via advection processes. Generally, under quiescent conditions, the meridional winds were southward during the daytime and shifted northward after sunset at Sanya (Figure 2c). On the superstorm day of 11 May 2024, the meridional winds changed directions between the southward and northward several times from 00:00-13:00 UT, with magnitudes exceeding ∼200 m/s. A crucial feature observed was the downward phase propagation in the meridional winds, indicating the presence of AGWs in the upper atmosphere.

Simultaneously, the vertical ion drifts underwent unique changes with clear quasiperiodic fluctuations. Large upward plasma drifts occurred several times from 00:00 UT to 13:00 UT, with maximum velocities of ∼50–70 m/s. In addition, downward plasma drifts were observed during 03:00–06:00 UT, 08:00–09:00 UT, and 10:30–13:00 UT, with maximum velocities of ∼15–20 m/s, with the largest velocity exceeding ∼60 m/s around sunset (10:30–13:00 UT). These special changes in vertical plasma drifts were significantly different from those reported by Fejer et al. (1995), who suggested that maximum drifts with a velocity of ∼20 m/s were usually upward and occurred at noon and sunset under quiescent conditions. These features were also observed on the reference day of 13 May 2024 when the vertical drifts were upward during the daytime and downward during the nighttime (Figure 2d). The magnetospheric electric fields can promptly penetrate into the equatorial ionosphere as a PPEF under southward IMF B_z excursions, which can enhance the upward plasma drifts during the daytime (Spiro et al., 1988). Although the geomagnetic storm entered the recovery phase after 03:00 UT when *Dst* started to recover, there were still significant recurrent southward IMF B_z excursions (Figure 1e). The recurrent larger upward plasma drifts generally corresponded to the southward IMF B_z excursions during 00:00-10:00 UT.

Furthermore, we analyzed the TEC variations along the longitude of 110° E in both hemispheres on 11 May 2024 and on the quiescent day of 8 May 2024 as well. As shown in Figure 3, the diurnal TEC variation with a peak during daytime and a small one during nighttime was observed in both hemispheres from the GNSS network on a quiescent day. It should be noted that the TEC on the reference day of 9 May 2024 for the simulation was not presented. The SYISR data were only available for half-day observations on both 8 and 9 May 2024. For TEC, it exhibited significant equatorial plasma bubbles on 9 May 2024. However, the selection of different reference days does not alter the major results of this study.

Compared to the reference day, unique features were observed in the TEC on this superstorm day (Figures 4a and 4b). The TECs showed not only multiple peaks but also daytime bite-outs between 00:00 and 13:00 UT at different latitudes on the superstorm day of 11 May 2024. Surprisingly, two humps usually seen in the daytime EIA structure disappeared. In particular, the TECs also manifested wavelike structures. The occurrence time of the TEC peaks was generally delayed with decreasing latitudes. For instance, the maximum peak in the Northern Hemisphere occurred progressively from ∼03:00 UT at higher latitudes (∼40°N) to ∼04:30 UT at lower latitudes (∼15°N). We calculated the phase speeds of these most evident TEC waves: 464.8 m/s during ∼03:00–04:30 UT, 936.2 m/s during ∼07:00–08:00 UT, and 656.8 m/s during ∼08:30–09:00 UT in the Northern Hemisphere; and 692.6 m/s

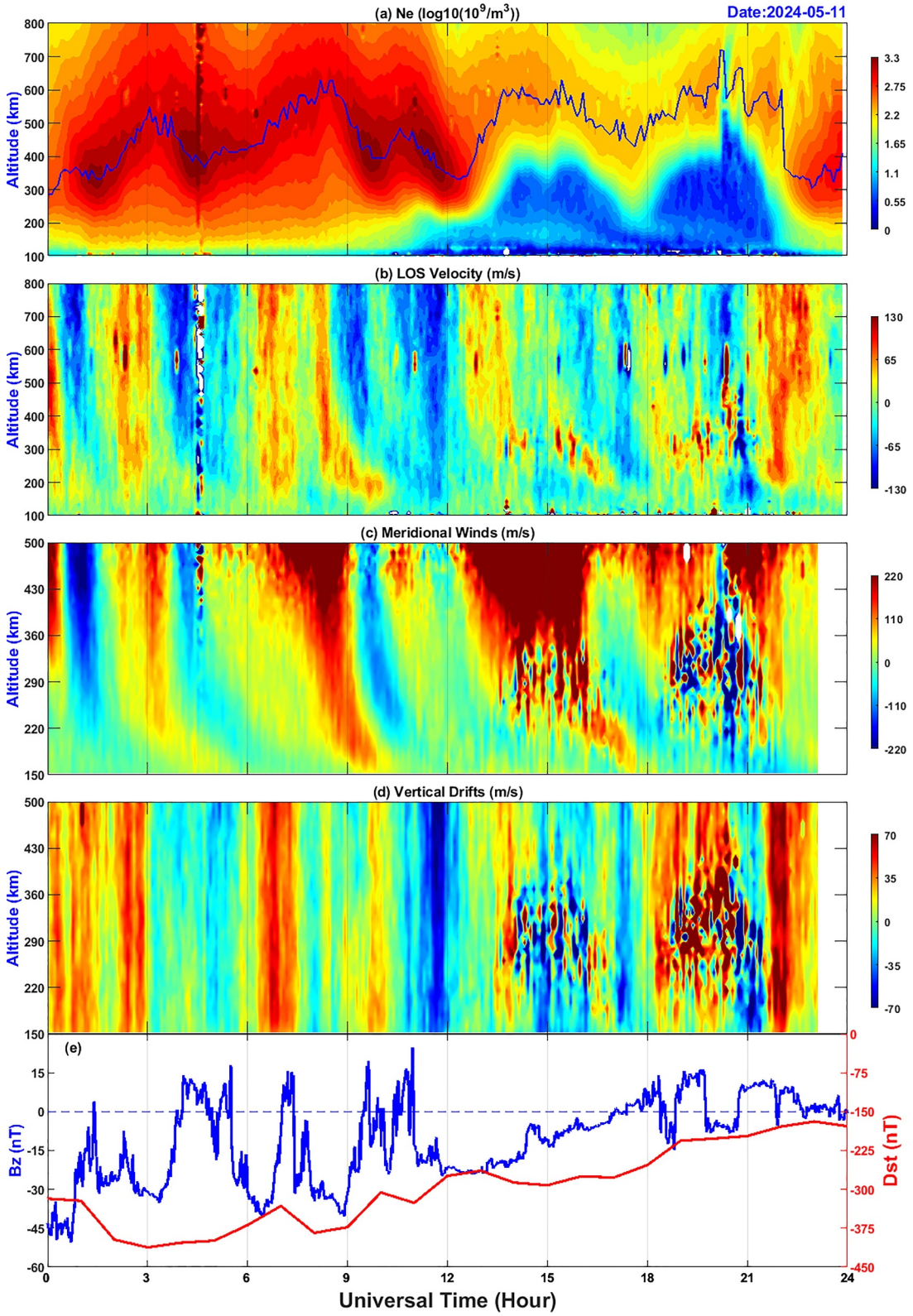

Figure 1.

during ~03:15–04:20 UT, 558.9 m/s during ~04:25–05:45 UT, and 928.0 m/s during ~08:45–09:20 UT in the Southern Hemisphere. The relative scarcity of TEC observations in the Southern Hemisphere may affect the velocity calculations. Nevertheless, they all fell within the typical velocity range for large-scale traveling ionospheric disturbances (LSTIDs), as the AGW phenomenon originated from auroral zones (Richmond, 1978).

In order to further analyze the physical processes underlying the abnormal ionospheric variations during this superstorm, we conducted simulations using the TIEGCM. Compared with the GEO TEC observations, as shown in Figures 4c and 4d, the simulations predicted similar TEC changes during 10–12 May 2024, despite some differences that will be discussed later. The TEC EIA with a clear crest in both hemispheres on 10 May and a single TEC peak in the Southern Hemisphere on 12 May were presented in the simulations and observations. Notably, on 11 May 2024, the observed TEC did not show a clear EIA structure but rather two or more TEC peaks at most latitudes, which were also reproduced in the simulated TEC. In addition, as shown in Figure 5, the simulated electron density, meridional winds, and vertical drifts at Sanya, exhibited similar characteristics to those observed by the SYISR. The simulated electron density displayed unique ionospheric changes without obvious diurnal variation at the F2 layer altitudes, similar to the SYISR observations. Multiple electron density peaks occurred on 11 May 2024, manifesting the wavelike structures. In addition, the simulated meridional winds and vertical plasma drifts showed features similar to those observed by SYISR. There were significant meridional wind disturbances, with downward phase propagation caused by AGWs observed in the meridional winds of different directions. Meanwhile, the obvious fluctuation was presented in the vertical plasma drifts. The large upward plasma drifts occurred several times from 00:00 UT to 13:00 UT. The strong downward drift velocity was also predicted around sunset (10:30–13:00 UT). It should be noted that the simulated peak height of electron density is higher than that observed by SYISR, which could be associated with the vertical plasma drifts caused by the overestimation of the electric fields, as discussed later. These results indicated that the TIEGCM simulation can be used to effectively analyze the physical processes underlying the unique ionospheric changes observed during the May 2024 superstorm.

Figure 6 shows the variations in the TEC, meridional winds, vertical plasma drifts, and vertical plasma drifts associated with disturbance dynamo from the TIEGCM along the longitude of 110°E on 11 May 2024. We can see that strong meridional wind disturbances and large upward $E \times B$ drifts occur recurrently during 00:00–13:00 UT, coinciding with multiple peaks in the simulated TEC. Strong southern B_z excursions recurred several times from 00:00 to 13:00 UT when enhanced Joule heating can induce strong multiple TADs in the polar region. These TADs can then propagate to lower latitudes and may even go cross the equator into the opposite hemisphere. The simulated meridional winds exhibited significant disturbances with maximum amplitudes of approximately 500 m/s, demonstrating strong TAD propagation characteristics. Concurrently, large upward vertical $E \times B$ drifts took place several times during period from 00:00 to 13:00 UT, generally corresponding to strong recurrent southward B_z excursions. This demonstrated that the large upward plasma drift oscillations might be associated with the PPEFs, which can enhance the upward plasma drifts during daytime and sunset (Spiro et al., 1988).

In addition, as mentioned above, the SYISR observations exhibited downward ion drifts during daytime and at sunset, with especially high velocities around sunset. As shown in Figure 6c, the simulated vertical drifts also had noticeable downward drift velocities from 09:00 UT to 14:00 UT. The disturbance dynamo electric fields (DDEFs) driven by the wind disturbance dynamo could occur a few hours after the beginning of the storm and last for several days (Blanc & Richmond, 1980), generally leading to downward plasma drifts during daytime and sunset (Fejer et al., 2008). We examined the vertical plasma drifts driven by the disturbance dynamo by a controlled run, as shown in Figure 6d. The plasma experienced a downward drift from 01:00 to 14:00 UT. The downward velocities were approximately 20 m/s during the daytime. Maximum velocities of ~100 m/s were observed around sunset, during which the SYISR observations also exhibited the largest downward ion drift velocities.

Figure 1. Variations in (a) electron density (*Ne*) and (b) line-of-sight (LOS) velocity (upward positive) from the SYISR zenith beam experiment, and (c) meridional winds (southward positive) and (d) vertical plasma drifts (upward positive) calculated from the SYISR multiple beam experiments as a function of universal time and altitude on the superstorm day of 11 May 2024. The interplanetary magnetic field (IMF) B_z in GSM coordinates, along with the geomagnetic activity index *Dst*, are plotted to indicate changes in geophysical conditions. The hmF2 is also shown by blue lines in panel (a). Note that a messy perturbation of the meridional winds and vertical ion drifts from 200 to 400 km during 14:00–17:00 UT and 19:00–22:00 UT was due to a small electron density resulting in low signal-to-noise ratio. As the duration of these echoes is relatively short, and their range is limited, these scattering echoes do not greatly impact the studying period of interest.

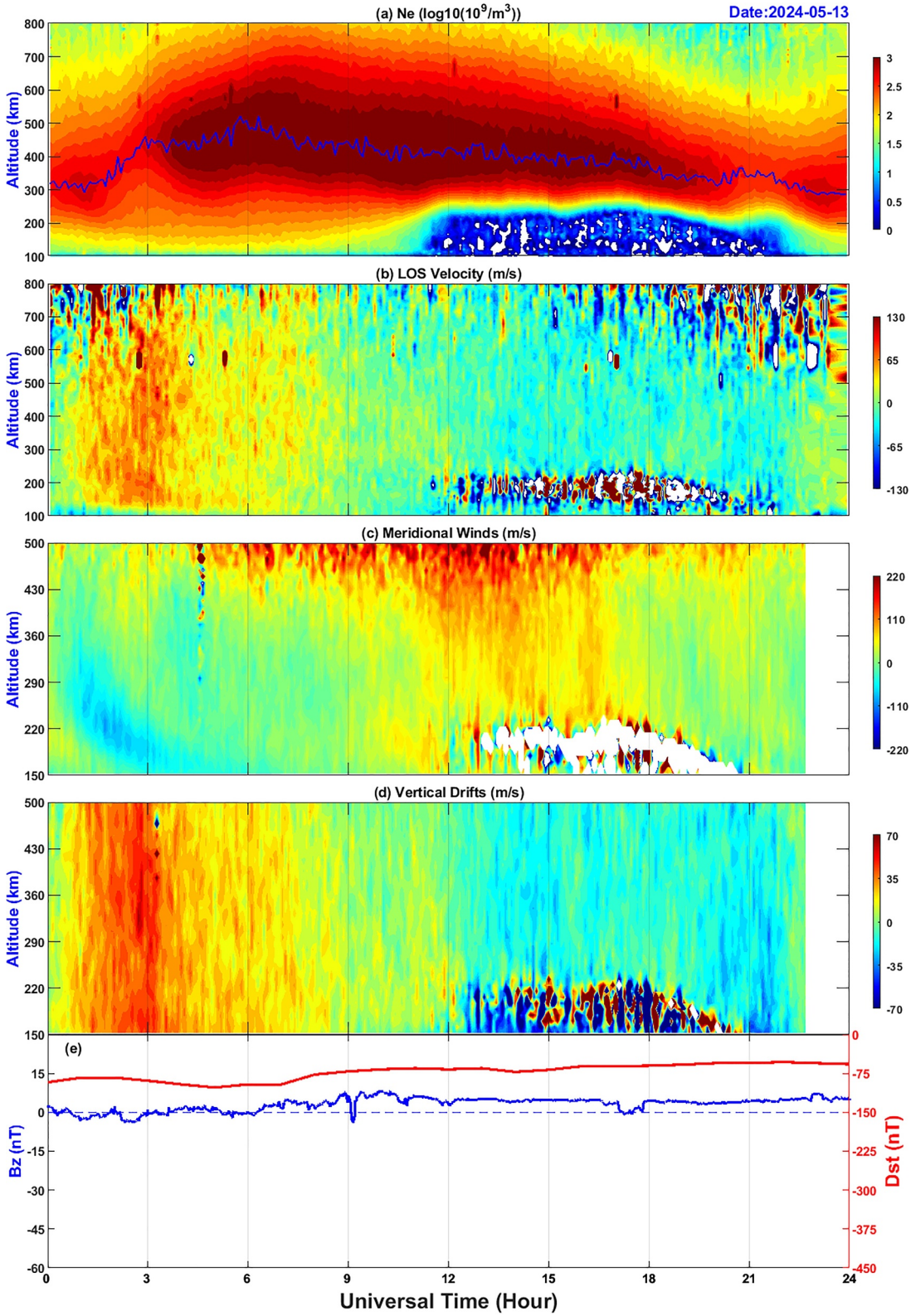

Figure 2. Same as Figure 1, but on the reference day of 13 May 2024. Note that the scatters of the meridional winds and vertical ion drifts from 150 to 250 km during 12:30–20:00 UT were due to a small electron density resulting in low signal-to-noise ratio.

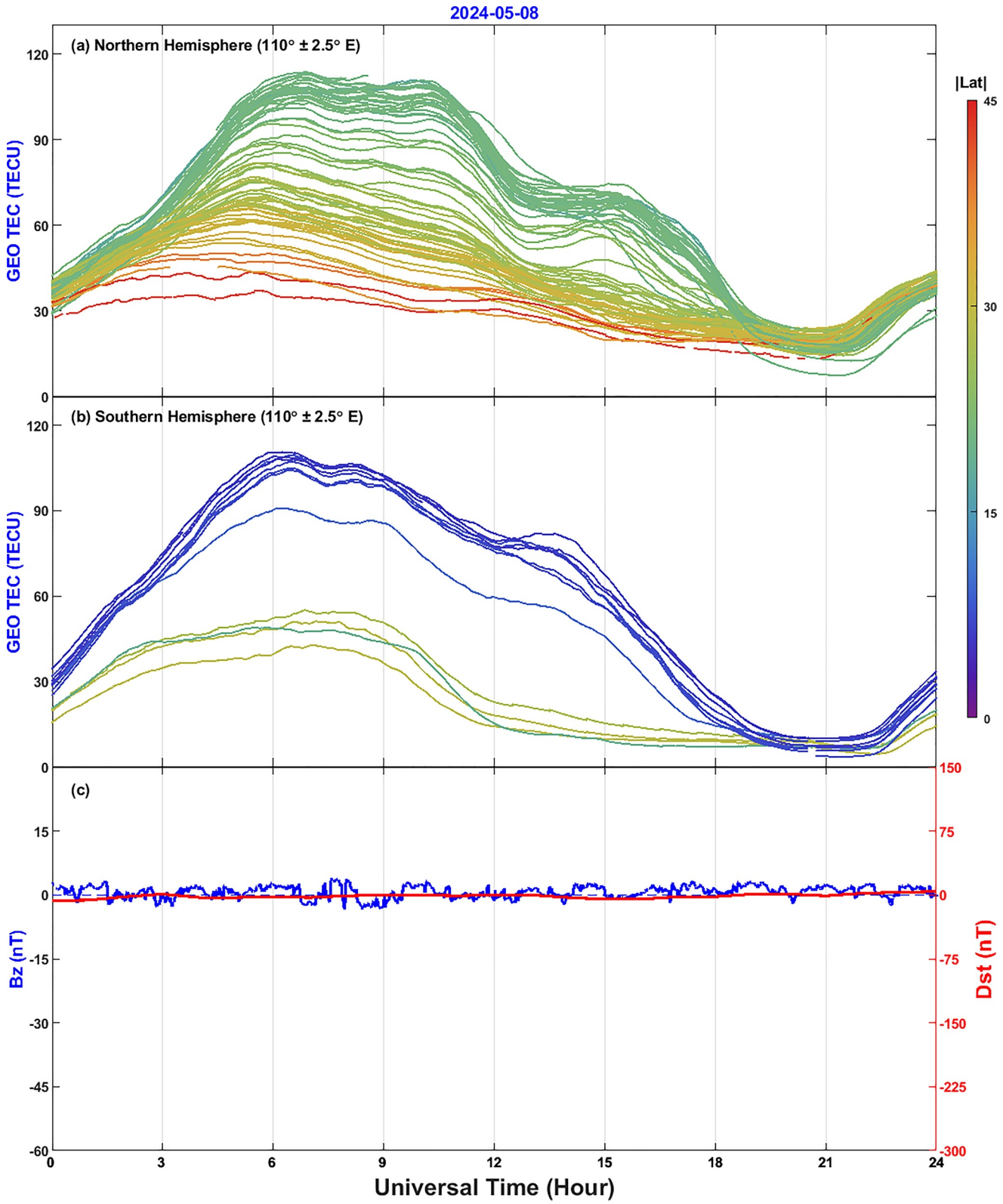

Figure 3. Daily variations of GEO total electron content (TEC) at the longitude of ∼110°E at different latitudes in the (a) Northern and (b) Southern Hemispheres on the quiescent day of 8 May 2024. The various colors of lines indicate the absolute values of the geographic latitudes. The IMF B_z in GSM coordinates, along with the geomagnetic activity index *Dst*, are plotted to indicate changes in geophysical conditions.

10.1029/2024AV001379

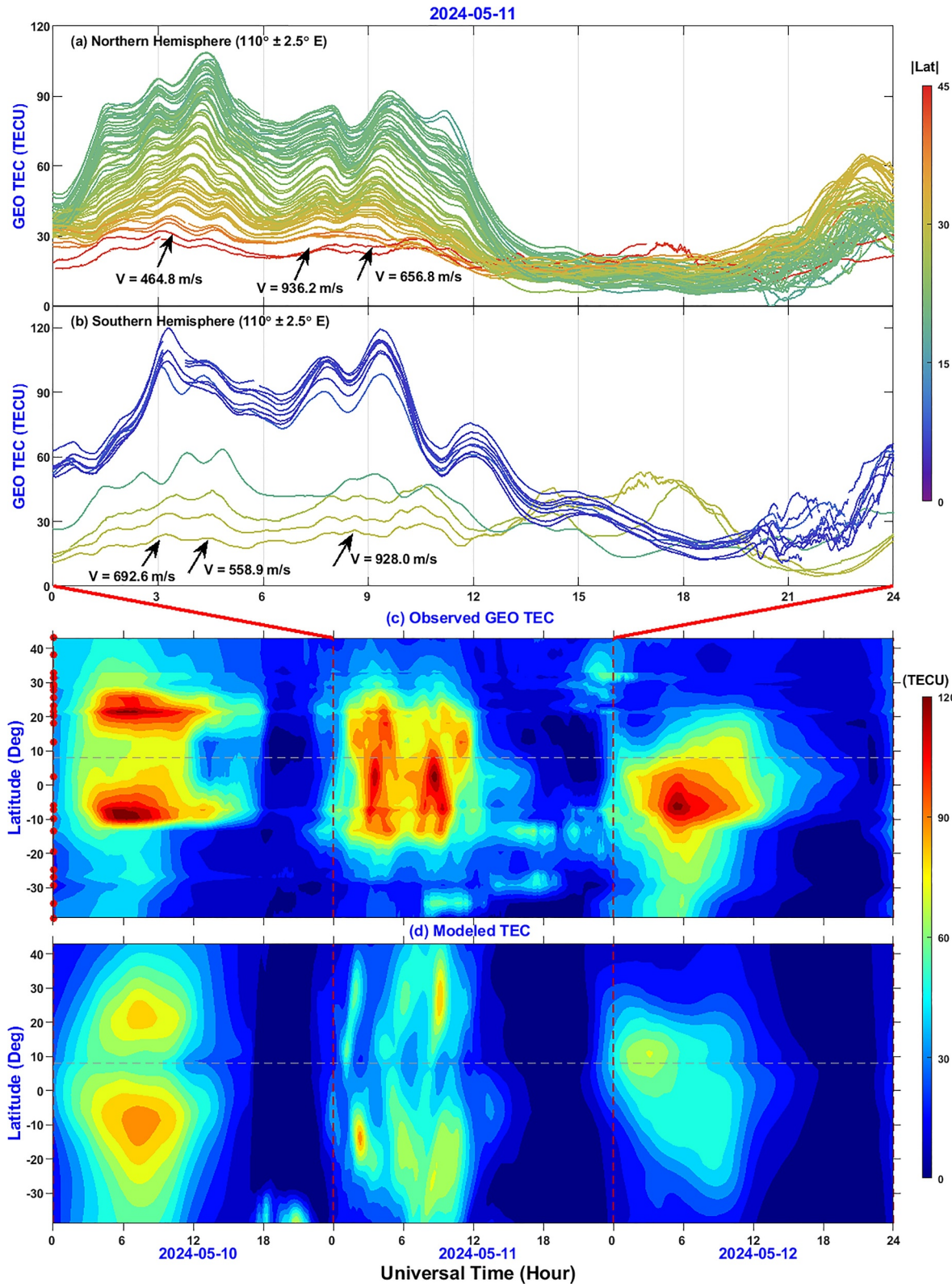

Figure 4. Daily variations in the GEO total electron content (TEC) at a longitude of ∼110°E at different latitudes in the (a) Northern and (b) Southern Hemispheres on 11 May 2024 and comparison of the TEC variations obtained from the (c) GEO satellites and (d) TIEGCM simulations as a function of IPP latitudes at a longitude of ∼110°E over the Asian sector from 10 to 12 May 2024. The various colors of the lines indicate the absolute values of the geographic latitude. The phase speed of the large-scale traveling ionospheric disturbances in the TEC is also marked in panels (a) and (b). The horizontal dashed line denotes the latitude of the geomagnetic equator at 110°E.

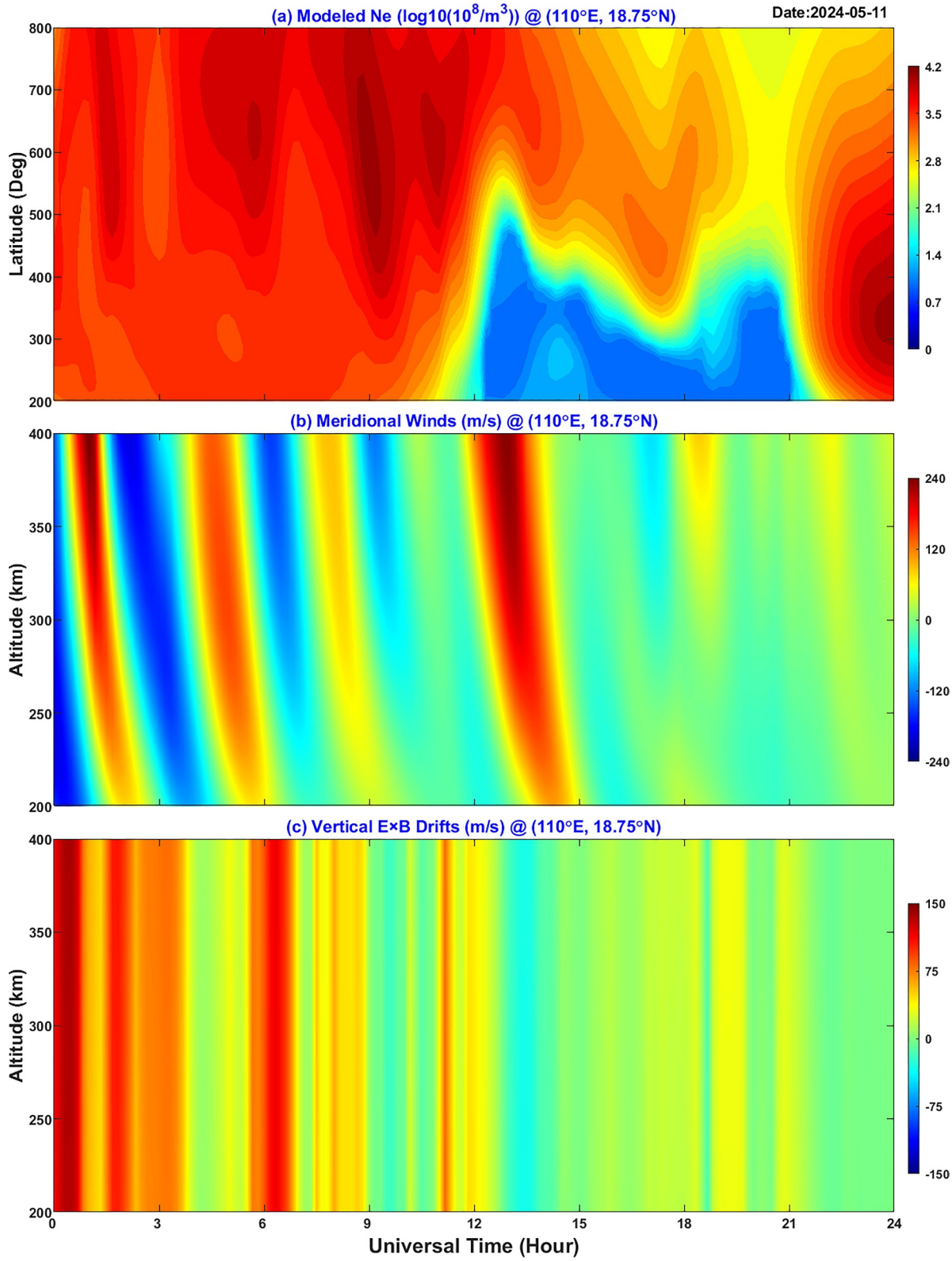

Figure 5. Simulated electron density (*Ne*), meridional winds (southward positive), and vertical $E \times B$ drifts (upward positive) as a function of universal time and altitude at Sanya from the TIEGCM on 11 May 2024.

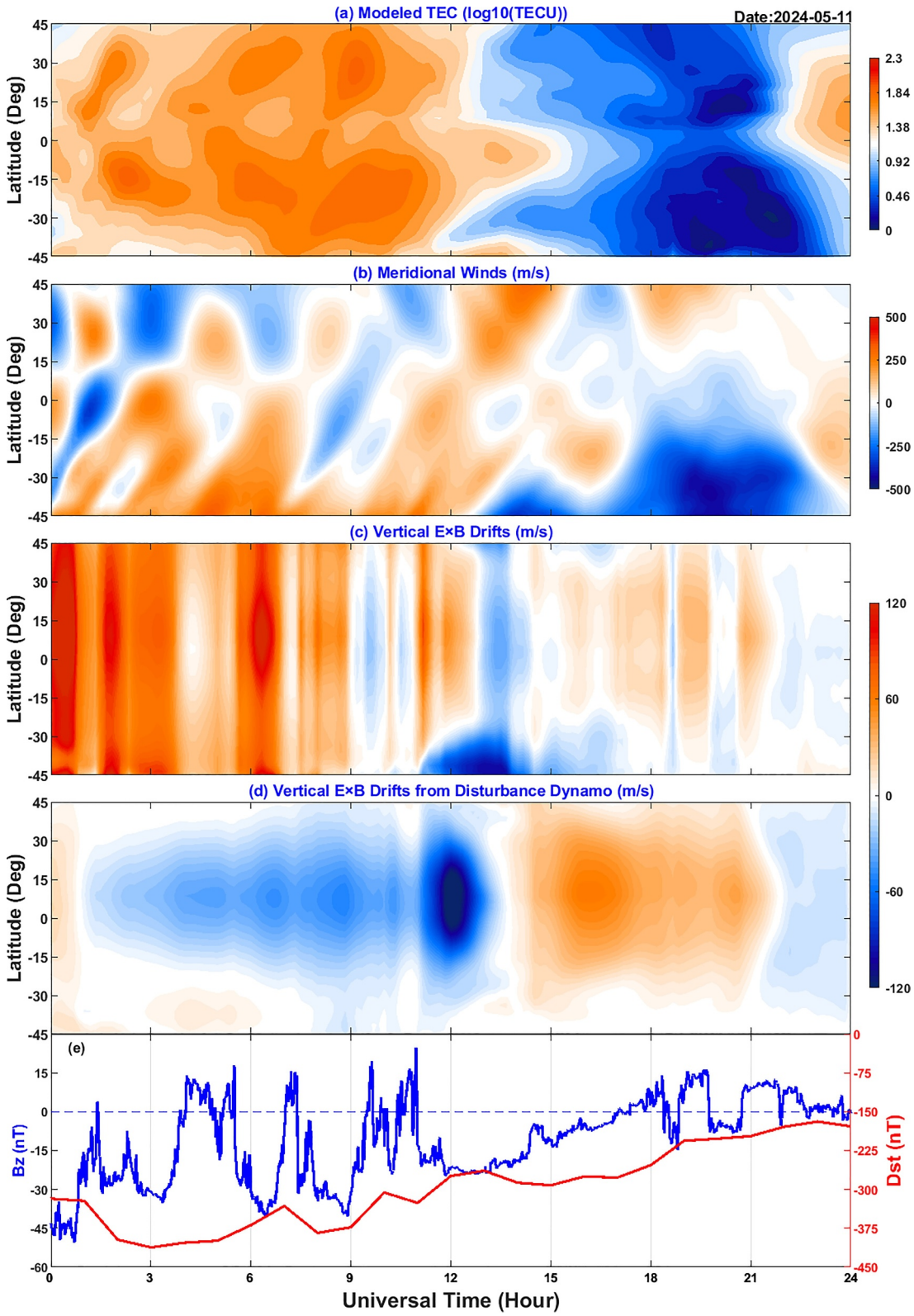

Figure 6. Simulated (a) total electron content, (b) meridional winds (southward positive), (c) vertical plasma drifts (upward positive), and (d) vertical plasma drifts associated with disturbance dynamo at an altitude of 300 km along the longitude of 110°E on 11 May 2024. See the text for more details. The IMF B_z in GSM coordinates, along with the geomagnetic activity index *Dst*, are plotted to indicate changes in geophysical conditions.

Furthermore, we analyzed their respective contributions to the TEC changes by running three controlled model simulations. As indicated in Figure 7, the simulated TEC on 11 May 2024 was lower than that on 9 May 2024 (quiet time) at the equator and low latitudes, except for one peak occurring at 03:00 UT and another at 09:00 UT at low latitudes. These TEC peaks generally corresponded to the positive effects of disturbed meridional winds associated with AGWs on the TEC. AGWs can carry wind surges, thereby uplifting (downlifting) the plasma and leading to TEC enhancements (decreases). The changes in the TEC with a maximum value of ∼±25 TECU were attributed to the meridional wind disturbances associated with the TADs (Figure 7b).

The vertical plasma drifts also greatly affected the TEC variations. Due to the oscillating PPEFs as induced by during the recurrent strong southern B_z excursions, the vertical $E \times B$ drifts displayed multiple large upward drifts during daytime and sunset, which resulted in multiple TEC enhancements at low and middle latitudes and TEC decreases at the magnetic equator during these periods. The maximum TEC decrease and TEC enhancement exceeded ∼25 TECU. However, disturbance electric fields, including PPEFs and DDEFs, can greatly affect the ionosphere. Particularly, during the storm recovery phase the DDEFs could be significant in modulating vertical plasma drifts and sometimes counteracting the effects of PPEFs. As shown in Figure 7d, the impact of the disturbance dynamo on vertical $E \times B$ drifts is substantial and cannot be overlooked. They can lead to TEC enhancements (decreases) at the equator and low latitudes (middle latitudes) during daytime and sunset. The effects of DDEFs were smaller than those of PPEFs during strong southern B_z excursions, which explains why the vertical plasma drifts mainly followed the features driven by PPEFs during daytime (Figure 7c). Around sunset, the disturbance dynamo became more pronounced, potentially outweighing the effects of the PPEF. These results demonstrated that the unique TEC changes were due to the contributions from disturbed meridional winds associated with AGWs and vertical plasma drifts related to the disturbance electric fields. The net changes in electric field disturbances were determined by the combined contributions of the PPEFs and DDEFs.

Themens et al. (2024) analyzed the high-latitude ionospheric evolution during the same superstorm of 10–11 May 2024 by utilizing TECs in conjunction with ISR and ionosonde observations. They reported the lifting of ionospheric plasma at mid-latitudes within the initial storm enhanced density region, where the peaks reached as high as ∼630 km and peak densities arose several times larger than that of the background conditions. And noted the LSTID-like oscillations occurred over North America during the initial phase of the storm, which could be also associated with the AGWs and disturbance electric fields. Further, Themens et al. (2024) found the complete absence of the F2-layer due to strong polar heating and composition changes on 11 May. Similarly, the present study revealed a negative storm in TECs (Figure 7a), while the TEC exhibited wave-like structures at low and middle latitudes. It should be noted that different ionospheric responses in the North American and Chinese sectors could be influenced by storm onset time, geomagnetic field configurations, and other effects. For example, disturbance electric fields may have different directions in the two sectors due to the local time differences at the same UT. Further investigation of the different ionospheric responses between North American and Chinese sectors is desired but is beyond the scope of this initial study.

Finally, it should be noted that there were still some discrepancies in the morphology produced by the model, despite its general ability to describe the abnormal ionospheric variations during the May 2024 superstorm. For instance, the TIEGCM overestimated the upward plasma drifts, producing peak speeds exceeding ∼120 m/s, whereas the SYISR observations showed peak velocities of ∼50–70 m/s. This overestimation may be related to the overestimation of the penetration of electric fields by the model, especially for large southward B_z cases, as discussed in previous studies (e.g., W. Wang et al., 2008, 2010). The penetration of high-latitude electric fields was approximately simulated by the TIEGCM with the Weimer model driven by solar wind and the IMF, although in this study, the TIEGCM was not self-consistently coupled with the magnetosphere and ring current models to address the shielding and overshielding processes. Nevertheless, the temporal variations in the observed vertical ion drift from the SYISR were generally consistent with the modeled plasma drift changes: that is, large daytime upward drifts occurred when the recurrent strong southward B_z excursions were present, and prominent downward drifts were observed around sunset. Thus, the TIEGCM model captured the temporal variability induced by the changes in the solar wind and IMF conditions during this superstorm and their impacts on the I-T System.

Additionally, the overestimation of high-latitude electric fields could also cause the overestimation of Joule heating and global neutral wind circulation and, in turn, disturbance dynamo effects (W. Wang et al., 2008). The morphology of the simulated TECs differed from that of the observed TECs (Figures 4c and 4d). The

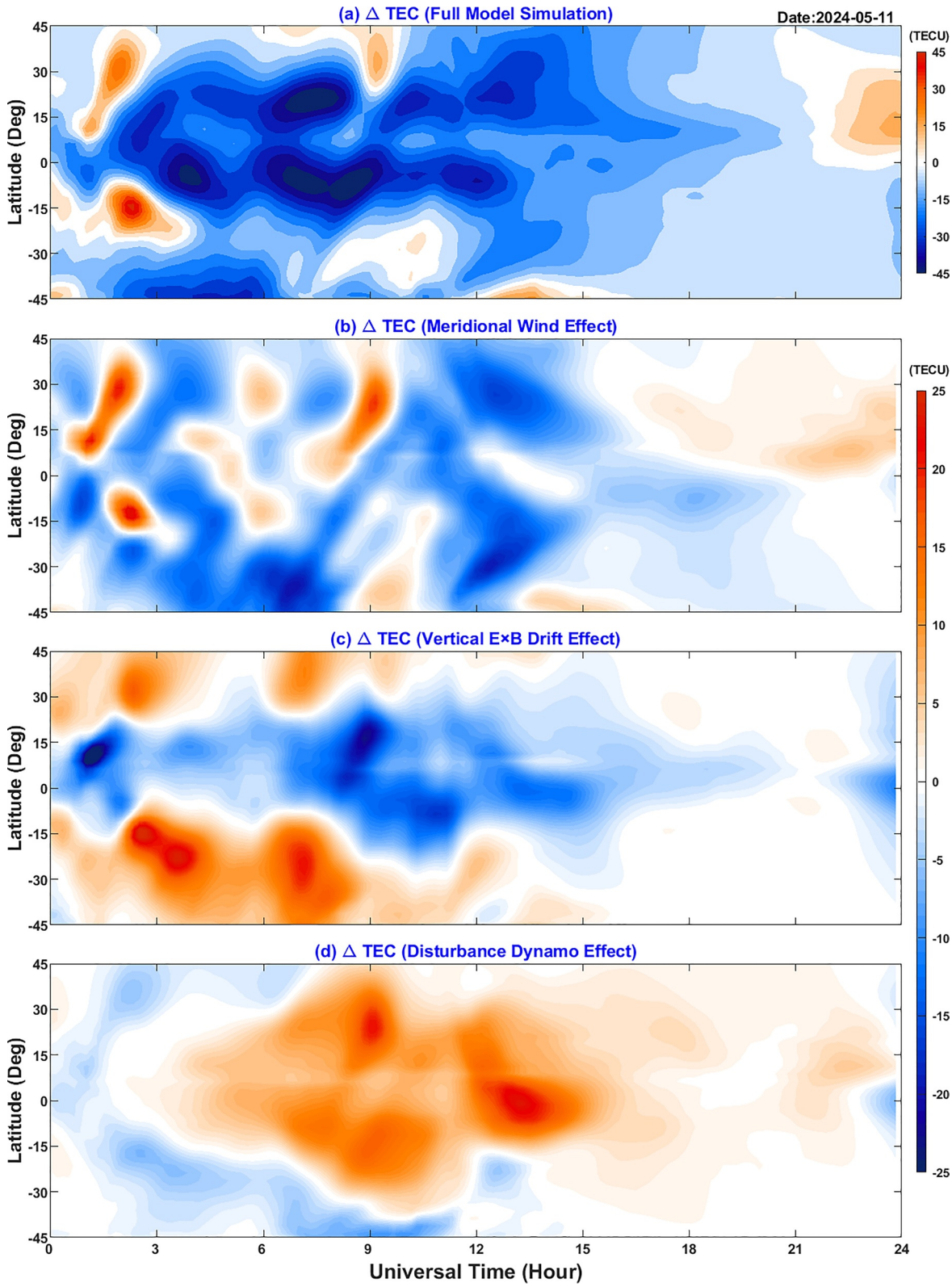

Figure 7. Changes in the simulated total electron content under (a) actual storm conditions (storm—quiet in Run 1) and with replacement of (b) meridional winds (Run 2–Run 1), or (c) vertical plasma drifts (Run 3–Run 1) or (d) disturbance dynamo (Run 4–Run 1) along the longitude of 110°E on 11 May 2024.

discrepancies in meridional winds and vertical plasma drifts between the observations and simulations may be associated with many factors. Lower atmospheric forces could also result in disparities between observations and simulations during storms (e.g., Lei et al., 2018). Also, the upper boundary of the TIEGCM is less than 1,000 km, whereas the observed TEC is the integrated content from the receiver up to the GEO satellite altitude (~36,000 km). The effects of the plasmasphere were neglected in the model. These aspects necessitate further investigation in the future.

4. Conclusion

Recently, the Chinese "Meridian Project" has offered robust ground-based observations for monitoring the ionosphere environment. In this study, we first used SYISR experiments and GEO TEC network measurements to analyze the ionospheric responses of the Asian sector to the May 2024 superstorm, the strongest storm in the preceding 20 years. The SYISR electron density and GEO TEC data exhibited abnormal ionospheric variations, displaying multiple peaks and wavelike structures. The estimated phase velocities of wavelike structures ranged from approximately 460 m/s to 940 m/s, which are characteristics of typical LSTIDs. The observed meridional winds had significant disturbances with maximum velocities exceeding ~200 m/s, accompanied by downward phase propagation associated with AGWs/TADs. Simultaneously, downward velocities around sunset and multiple large upward velocities during daytime with peak values of ~50–70 m/s, were observed in the vertical ion drifts from SYISR measurements. The TIEGCM also predicted similar ionospheric changes, attributing these variations to the contributions from disturbed meridional winds related to AGWs and plasma drifts driven by DDEFs and recurrent PPEFs under southern B_z conditions. These comprehensive observations and simulations demonstrated that the interactions among actions among AGWs, penetration electric fields and the disturbance dynamo were responsible for the abnormal ionospheric changes during this superstorm. This study provided an important insight for understanding the relative effects of disturbance electric fields, neutral wind disturbances, and their interactions during strong geomagnetic storms.

Conflict of Interest

The authors declare no conflicts of interest relevant to this study.

Data Availability Statement

The Beidou GEO TEC data are provided by the USTC Beidou Ionospheric Monitoring Network and the IGS network from NASA CDDIS (https://cddis.nasa.gov). We acknowledge NOAA National Centers for Environmental Information (NCEI) (https://www.ngdc.noaa.gov/dscovr) for solar wind and IMF B_z and World Data Center for Geomagnetism, Kyoto (https://wdc.kugi.kyoto-u.ac.jp/) for *Dst*. The Beidou GEO TEC, SYISR, and TIEGCM simulation data are available from the Science Data Bank (ScienceDB) via https://www.scidb.cn/en/s/Ij6nai (F. Huang, 2024).

References

Blanc, M., & Richmond, A. D. (1980). The ionospheric disturbance dynamo. *Journal of Geophysical Research*, *85*(A4), 1669–1686. https://doi.org/10.1029/JA085IA04P01669

Buonsanto, M. J. (1999). Ionospheric storms—A review. *Space Science Reviews*, *88*(3/4), 563–601. https://doi.org/10.1023/A:1005107532631

Coster, A. J., Erickson, P. J., Lanzerotti, L. J., Zhang, Y., & Paxton, L. J. (2021). *Space Weather Effects and Applications, Space Physics and Aeronomy Collection*, *Geophysical Monograph 262* (Vol. 5). American Geophysical Union and Wiley. https://doi.org/10.1002/9781119815570

Dang, T., Li, X., Luo, B., Li, R., Zhang, B., Pham, K., et al. (2022). Unveiling the space weather during the Starlink satellites destruction event on 4 February 2022. *Space Weather*, *20*(8), e2022SW003152. https://doi.org/10.1029/2022SW003152

Dang, T., Luan, X., Lei, J., Dou, X., & Wan, W. (2016). A numerical study of the interhemispheric asymmetry of the equatorial ionization anomaly in solstice at solar minimum. *Journal of Geophysical Research: Space Physics*, *121*(9), 9099–9110. https://doi.org/10.1002/2016JA023012

Fejer, B. G., de Paula, E. R., Heelis, R. A., & Hanson, W. B. (1995). Global equatorial ionospheric vertical plasma drifts measured by the AE-E satellite. *Journal of Geophysical Research*, *100*(A4), 5769–5776. https://doi.org/10.1029/94JA03240

Fejer, B. G., Jensen, J. W., & Su, S.-Y. (2008). Seasonal and longitudinal dependence of equatorial disturbance vertical plasma drifts. *Geophysical Research Letters*, *35*(20), L20106. https://doi.org/10.1029/2008GL035584

Gonzalez, W. D., Joselyn, J. A., Kamide, Y., Kroehl, H. W., Rostoker, G., Tsurutani, B. T., & Vasyliunas, V. M. (1994). What is a geomagnetic storm? *Journal of Geophysical Research*, *99*(A4), 5771–5792. https://doi.org/10.1029/93JA02867

Huang, C.-S., Foster, J. C., Goncharenko, L. P., Erickson, P. J., Rideout, W., & Coster, A. J. (2005). A strong positive phase of ionospheric storms observed by the Millstone Hill incoherent scatter radar and global GPS network. *Journal of Geophysical Research*, *110*(A6), A06303. https://doi.org/10.1029/2004JA010865

Acknowledgments

This work was supported by the National Natural Science Foundation of China (42188101), the Project of Stable Support for Youth Team in Basic Research Field, CAS (YSBR-018), the B-type Strategic Priority Program of the Chinese Academy of Sciences (XDB0780000), the International Partnership Program Of Chinese Academy of Sciences (Grant 183311KYSB20200003) and the International Space Science Institute (ISSI) in Bern and Beijing, through ISSI International Team project #511 (Multi-Scale Magnetosphere-Ionosphere-Thermosphere Interaction). X. Yue acknowledges the support of the National Natural Science Foundation of China (42425403). F. Huang acknowledges the support of the National Natural Science Foundation of China (42274195), the National Key R&D Program of China (2022YFF0504400), the USTC Research Funds of the Double First-Class Initiative (YD2080002013) and the Joint Open Fund of Mengcheng National Geophysical Observatory (MENGO-202408). SRZ was supported by US NSF awards AGS-2033787, AGS-2149698, and AGS-1952737 and NRL Grants N00014-24-1-2122 and N00014-23-1-2160. X. Luan acknowledges the support of the National Natural Science Foundation of China (42174193). The authors acknowledge the data resources from the Chinese Meridian Project and the National Space Science Data Center, National Science and Technology Infrastructure of China (http://www.nssdc.ac.cn/eng/). Numerical computations were performed at Hefei Advanced Computing Center.

Huang, F. (2024). Interplay of gravity waves and disturbance electric fields to the abnormal ionospheric variations during the 11 May 2024 superstorm [Dataset]. *Science Data Bank*. https://doi.org/10.57760/sciencedb.09588

Huang, F., Lei, J., & Dou, X. (2017). Daytime ionospheric longitudinal gradients seen in the observations from a regional BeiDou GEO receiver network. *Journal of Geophysical Research: Space Physics*, *122*(6), 6552–6561. https://doi.org/10.1002/2017JA023881

Huang, F., Lei, J., Dou, X., Luan, X., & Zhong, J. (2018). Nighttime medium-scale traveling ionospheric disturbances from airglow imager and Global Navigation Satellite Systems observations. *Geophysical Research Letters*, *45*(1), 31–38. https://doi.org/10.1002/2017GL076408

Huang, F., Lei, J., Luan, X., Li, G., Wang, Y., Zhu, Y., et al. (2023). Dynamic processes associated with prominent ionospheric variations in a narrow longitudinal zone near the EIA crest region as revealed by ICON satellite and ground Beidou receiver observations over South Asia. *Journal of Geophysical Research: Space Physics*, *128*(10), e2023JA031981. https://doi.org/10.1029/2023JA031981

Jin, H., Yan, C., Yang, G., Huang, F., Xie, H., Zhao, X., et al. (2022). Interaction between equatorial to low-latitude postmidnight F-region irregularities and LSTIDs in China during geomagnetic disturbances based on ground-based instruments. *Journal of Geophysical Research: Space Physics*, *127*(6), e2022JA030286. https://doi.org/10.1029/2022JA030286

Lei, J., Huang, F., Chen, X., Zhong, J., Ren, D., Wang, W., et al. (2018). Was magnetic storm the only driver of the long-duration enhancements of daytime total electron content in the Asian-Australian sector between 7 and 12 September 2017? *Journal of Geophysical Research: Space Physics*, *123*(4), 3217–3232. https://doi.org/10.1029/2017JA025166

Lei, J., Wang, W., Burns, A. G., Solomon, S. C., Richmond, A. D., Wiltberger, M., et al. (2008). Observations and simulations of the ionospheric and thermospheric response to the December 2006 geomagnetic storm: Initial phase. *Journal of Geophysical Research*, *113*(A1), A01314. https://doi.org/10.1029/2007JA012807

Lin, C. H., Richmond, A. D., Liu, J. Y., Yeh, H. C., Paxton, L. J., Lu, G., et al. (2005). Large-scale variations of the low-latitude ionosphere during the October–November 2003 superstorm: Observational results. *Journal of Geophysical Research*, *110*(A9), A09S28. https://doi.org/10.1029/2004JA010900

Liu, H.-L., & Vadas, S. L. (2013). Large-scale ionospheric disturbances due to the dissipation of convectively generated gravity waves over Brazil. *Journal of Geophysical Research: Space Physics*, *118*(5), 2419–2427. https://doi.org/10.1002/jgra.50244

Luan, X. (2021). Equatorial ionization anomaly variations during geomagnetic storms. In C. Huang, G. Lu, Y. Zhang, & L. J. Paxton (Eds.), *Ionosphere dynamics and Applications*. https://doi.org/10.1002/9781119815617.ch13

Ma, G., & Maruyama, T. (2006). A super bubble detected by dense GPS network at East Asian longitudes. *Geophysical Research Letters*, *33*(21), L21103. https://doi.org/10.1029/2006GL027512

Mannucci, A. J., Tsurutani, B. T., Abdu, M. A., Gonzalez, W. D., Komjathy, A., Echer, E., et al. (2008). Superposed epoch analysis of the dayside ionospheric response to four intense geomagnetic storms. *Journal of Geophysical Research*, *113*(A3), A00A02. https://doi.org/10.1029/2007JA012732

McNamara, L. F. (1991). *The ionosphere: Communications, surveillance, and direction finding*. Krieger Publishing Company.

Mendillo, M. (2006). Storms in the ionosphere: Patterns and processes for total electron content. *Reviews of Geophysics*, *44*(4), RG4001. https://doi.org/10.1029/2005RG000193

Prölss, G. W. (1993). Common origin of positive ionospheric storms at middle latitudes and the geomagnetic activity effect at low latitudes. *Journal of Geophysical Research*, *98*(A4), 5981–5991. https://doi.org/10.1029/92JA02777

Prölss, G. W. (1995). Ionospheric F-region storms. In H. Volland (Ed.), *Handbook of atmospheric electrodynamics* (pp. 195–248). CRC Press.

Richmond, A. D. (1978). Gravity wave generation, propagation, and dissipation in the thermosphere. *Journal of Geophysical Research*, *83*(A9), 4131–4145. https://doi.org/10.1029/JA083iA09p04131

Richmond, A. D., & Lu, G. (2000). Upper-atmospheric effects of magnetic storms: A brief tutorial. *Journal of Atmospheric and Solar-Terrestrial Physics*, *62*(12), 1115–1127. https://doi.org/10.1016/S1364-6826(00)00094-8

Richmond, A. D., & Roble, R. G. (1979). Dynamic effects of aurora generated gravity waves on the mid-latitude ionosphere. *Journal of Atmospheric and Terrestrial Physics*, *41*(7–8), 841–852. https://doi.org/10.1016/0021-9169(79)90127-2

Skone, S., & Yousuf, R. (2007). Performance of satellite-based navigation for marine users during ionospheric disturbances. *Space Weather*, *5*(1), S01006. https://doi.org/10.1029/2006SW000246

Spiro, R., Wolf, R., & Fejer, B. G. (1988). Penetrating of high-latitude-electric-field effects to low latitudes during SUNDIAL 1984. *Annales Geophysicae*, *6*, 39–49.

Themens, D. R., Elvidge, S., McCaffrey, A., Jayachandran, P. T., Coster, A., Varney, R. H., et al. (2024). The high latitude ionospheric response to the major May 2024 geomagnetic storm: A synoptic view. *Geophysical Research Letters*, *51*(19), e2024GL111677. https://doi.org/10.1029/2024GL111677

Wang, C., Xu, J., Chen, Z., Li, H., Feng, X., Huang, Z., & Wang, J. (2024). China's ground-based space environment monitoring network—Chinese Meridian Project (CMP). *Space Weather*, *22*(7), e2024SW003972. https://doi.org/10.1029/2024SW003972

Wang, C., Xu, J., Liu, L., Xue, X., Zhang, Q., Hao, Y., et al. (2023). Contribution of the Chinese Meridian Project to space environment research: Highlights and perspectives. *Science China Earth Sciences*, *66*(7), 1423–1438. https://doi.org/10.1007/s11430-022-1043-3

Wang, W., Lei, J., Burns, A. G., Solomon, S. C., Wiltberger, M., Xu, J., et al. (2010). Ionospheric response to the initial phase of geomagnetic storms: Common features. *Journal of Geophysical Research*, *115*(A7), A07321. https://doi.org/10.1029/2009JA014461

Wang, W., Lei, J., Burns, A. G., Wiltberger, M., Richmond, A. D., Solomon, S. C., et al. (2008). Ionospheric electric field variations during a geomagnetic storm simulated by a coupled magnetosphere ionosphere thermosphere (CMIT) model. *Geophysical Research Letters*, *35*(18), L18105. https://doi.org/10.1029/2008GL035155

Weimer, D. R. (2005). Improved ionospheric electrodynamic models and application to calculating Joule heating rates. *Journal of Geophysical Research*, *110*(A5), A05306. https://doi.org/10.1029/2004JA010884

Yue, X., Wan, W., Ning, B., & Jin, L. (2022). An active phased array radar in China. *Nature Astronomy*, *6*(5), 619. https://doi.org/10.1038/s41550-022-01684-1

Yue, X., Wan, W., Ning, B., Jin, L., Ding, F., Zhao, B., et al. (2022). Development of the Sanya incoherent scatter radar and preliminary results. *Journal of Geophysical Research: Space Physics*, *127*(8), e2022JA030451. https://doi.org/10.1029/2022JA030451

Zhang, N., Yue, X., Cai, Y., Wang, J., Li, M., Ding, F., & Ning, B. (2024). F Region neutral wind and electric field measured by SYISR and evaluation. *Journal of Geophysical Research: Space Physics*, *129*(5), e2024JA032514. https://doi.org/10.1029/2024JA032514